THE JOURNAL OF PHYSICAL CHEMISTRY C

Article

pubs.acs.org/JPCC

Ultrathin Anodic Aluminum Oxide Membranes for Production of Dense Sub-20 nm Nanoparticle Arrays

U. Malinovskis,[†] R. Poplausks,[†] I. Apsite,[†] R. Meija,[†] J. Prikulis,[†] F. Lombardi,[‡] and D. Erts*[,†]

[†]Institute of Chemical Physics, University of Latvia, 19 Raina Boulevard, LV-1586 Riga, Latvia

[‡]MC2, Quantum Device Physics Laboratory, Chalmers University of Technology, SE-41296 Gothenburg, Sweden

ABSTRACT: We present a systematic study of membrane structure (pore diameter and arrangement) in anodized aluminum oxide (AAO) layers obtained by anodization voltages 8−20 V in sulfuric and 15−40 V in oxalic acid electrolyte solutions. Anodization of bulk aluminum in sulfuric acid at 10 V potential was found to be optimal for production or ultrathin freestanding membranes with pore diameter in sub-20 nm range. The developed process with slow electrochemical reaction results in AAO membranes with thickness below 70 nm. The minimum required time for formation of continuous AAO membrane was determined and influence of electrolyte concentration on pore diameter in membrane after barrier layer removal analyzed. Finally, we demonstrate a method of membrane transfer onto a different surface and using it for masked deposition of dense nanoparticle arrays with diameters below 20 nm.

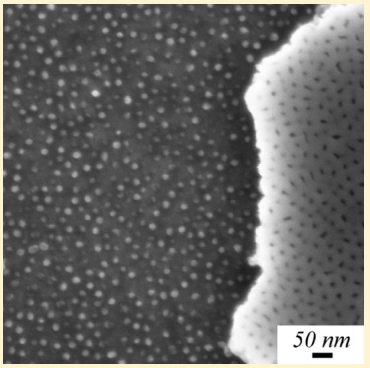

INTRODUCTION

Nanoporous anodized aluminum oxide (AAO) membranes persist to attract much attention due to their highly ordered porous structure, variable range of pore diameter and high density[1−3] although these surface features of AAO have been known for more than six decades.[4] AAO membranes are widely used for synthesis of nanowire and nanotube arrays, for filtration, as sensors, catalysts, patterning (evaporation and etching masks), and other applications.[1,5] Ultrathin AAO membranes were recently used as masks for production of nanoparticle arrays on different surfaces.

The membrane morphology can be controlled by anodization voltage and the type of electrolyte used. The pore diameter decreases nearly linearly with decreased anodization voltage.[2−4,6] However, this generally accepted rule breaks down at voltages below 5 V and the pore diameter may actually increase after further reduction of anodization voltage.[7] This suggests that the processes of membrane growth at low voltages (∼10 V) are different from regular cell formation at higher potentials.

In the case of electrically conductive substrates, for example, silicon or indium tin oxide, a thin layer of Al can be deposited and subsequently anodized.[3,8] Use of ultrathin AAO masks on other surfaces requires fabrication of free-standing membranes.[9−11] Various techniques of mask transfer, including coverage with a polymer transport substrate, which is afterward dissolved, have been developed.[9,10] AAO masks with pore diameters of 60−100 nm and thickness of 200−700 nm prepared in oxalic acid electrolyte solution at anodization voltage of 40 V yield nanoparticles with diameters of 50−80 nm.[12,13] Production of smaller nanoparticles, for example, for quantum dot applications, is more complicated and requires manipulation of ultrathin AAO masks with pore diameters below 20 nm and membrane-thickness to pore-width aspect ratio 10 or smaller.[14] Membranes with higher aspect ratio are less suitable for masked deposition because the sputtered material accumulates on membrane and does not reach the target surface. The limiting factor from the other end is the mechanical strength of porous AAO and membranes thinner than ∼100 nm are difficult to handle.

In a recent work by Wu et al., ultrathin AAO membranes with pore diameter below 20 nm and thickness 80 nm have been fabricated by Al anodization in sulfuric acid at a potential of 25−40 V.[10] This was achieved only after decreasing the reaction speed by cooling the electrolyte to −20 °C and adding modulators to the solution. For relatively thick AAO membranes the pores can be grown to a well-ordered honeycomb structure. However, the process parameter (electrolyte concentration, anodization voltage, and so forth) influence on pore structure in limiting cases of ultrathin masks has been much less studied.

In this work, low-anodization voltages and consequently low reaction speeds were used for reproducible synthesis of AAO membranes with thickness below 70 nm and pore diameters below 20 nm. Here we extend the initial study by our group[15] and systematically analyze the influence of electrolyte concentration and anodization voltages on membrane morphology. We have significantly improved the ultrathin membrane transfer method and found optimal parameters for nanoparticle deposition mask production. We demonstrate this by creating dense Cr nanoparticle arrays with 16 nm particle diameter on a Si surface. To our knowledge the reported smallest nanoparticles produced by masked deposition

Received: December 27, 2013
Revised: March 10, 2014

dx.doi.org/10.1021/jp412689y | J. Phys. Chem. C XXXX, XXX, XXX−XXX

technique through AAO membrane have 17 nm average diameter.[10] The presented recipe fills the gap in 10−20 nm range where top-down (lithography) and bottom-up (colloid synthesis) methods become increasingly difficult. Moreover, the change of nanoparticle material for particular applications is straightforward, for example, in a recent work by our group similar size Ag nanoparticles were used on glass surface for plasmonic applications.[16]

EXPERIMENTAL SECTION

Ultrathin AAO membranes were prepared by two-stage anodization of high-purity 0.35 mm thick aluminum foil (99.999% GoodFellow, Cambridge) in sulfuric (0.3−1.3 mol/L) acid or oxalic (0.3 mol/L) acid by applying direct current (dc) voltage. After degreasing in acetone, aluminum sheets (18 mm × 9 mm × 0.35 mm) were annealed in vacuum at a 450 °C for 2 h and slowly cooled to room temperature. Annealed aluminum sheets were electropolished under a constant voltage of 10 V at room temperature in a mixed solution of perchloric acid (60% $HClO_4$) and ethanol (96% EtOH) in a volume ratio of 1:4.[17] The electropolished aluminum sheets were first anodized at room temperature for 2 h in sulfuric acid or oxalic acid under a constant voltage in a two-electrode cell with a platinum cathode. The resulting oxide layer was removed with a 3.5% (vol) solution of H_3PO_4 and 4.5% CrO_3 at 70 °C.[18] A second anodization step was performed at room temperature under the same conditions as the first anodization. The anodization time minimum 25−30 s was predetermined for each sample type where stabilization of anodization current occurs (Figure 1), which corresponds to beginning of steady state growth of porous alumina.[19]

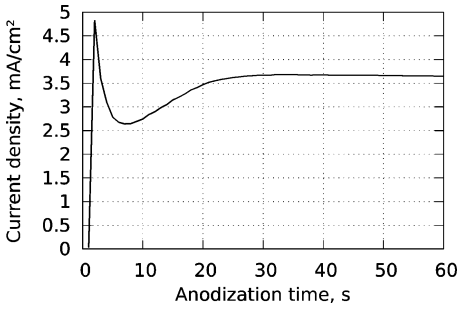

Figure 1. Current−time curve obtained during second anodization using 10 V potential in 0.7 M sulfuric acid.

The ultrathin AAO surface formed during the second anodization was coated with a layer of poly(methyl methacrylate) PMMA 950k in 6% anisole solution (MicroChem). The sample was left for 14 h to allow the solvent to evaporate. Thereafter the PMMA layer was reinforced by a 1−2 mm coating of paraffin.

The aluminum substrate was then removed by floating the sample on the surface of a mixture solution of 0.37 M $CuCl_2$/1 M HCl and 10 wt % $FeCl_3$ in volume ratio 1:3. A tiny amount (0.1%) nonionic surfactant Triton X-100 was added to the above etching mixture. The barrier layer was selectively removed by placing the composite membrane on the surface of a 5 wt % H_3PO_4 solution at room temperature. The ultrathin AAO membrane was then transferred onto plasma cleaned cover glass or Si surface and left to dry for 14 h (overnight). Paraffin was blown away with hot air and PMMA layer was removed by a flow of oxygen at 500 °C.

Chrome (Ag, Au, and other materials not shown here) nanoparticles were deposited on substrate surfaces using ion beam-based GATAN Precision Etching and Coating System (Model 682 PECS). After 20−30 nm thick metal layer deposition, AAO mask was removed using adhesive thermal release tape.

Thickness of the transferred AAO was measured with atomic force microscope (Asylum Research MFP-3D Bio, AC mode). Field-emission scanning electron microscope (SEM, Hitachi 4800 or Carl Zeiss SUPRA 60 VP) was used for observation of the ultrathin AAO and metal nanoparticles. For pore characterization the SEM images were processed (brightness and contrast correction) and analyzed (Voronoi diagrams) with ImageJ software.[20] The pore diameter was determined by averaging measurements from 100 pores obtained by analysis of intensity in SEM images with the intensity threshold values set to visually match the structure of full pores (excluding incomplete, double and branched ones).

RESULTS AND DISCUSSION

Anodization at Low Voltages. With the initial goal of finding process parameters for production of membranes with smallest pores and highest densities while maintaining suitable thickness-diameter aspect ratio for mask deposition, anodization was done at lower potentials (8−12 and 15 V sulfuric and oxalic acid electrolyte solution, respectively) compared to 40 and 25 V typically reported in literature.[2,9] We found that these values did indeed yield ultrathin masks, which could be produced at room temperature. However, they lack the prominent honeycomb structure one typically expects from AAO masks. To illustrate this, AAO layers were synthesized using two-step anodization process of Al sheets in a 0.3 M oxalic acid under different anodization voltages with 45 s anodization time.

In contrast to "typical" medium anodization voltage samples, where large areas are covered by nearly periodic structure (Figure 2a,b), the arrangement of pores in low anodization voltage samples (Figure 2d) has a short-range ordered nature. The pore diameter and cell size at the initial stage of AAO layer formation, which is of interest in present study, decreases with lower anodization voltage, which is in good agreement with earlier observations for steady growth of thick membranes.[6,21] Pore diameter of AAO decreased from 39 to 16 nm and cell size from 102 nm (standard deviation 5%) to 43 nm (standard deviation 23%). Moreover, pores of AAO, prepared at 15 V were more variable in shape, some pores were branched or paired (distance between pores were equal or smaller than pore diameter). To establish the degree of ordering of pores, Voronoi diagrams[22,23] were constructed and superimposed on SEM images (Figure 2c,e). Pores prepared under 40 V have six neighbors (are hexagonally ordered) in ∼1 μm^2 large domains (Figure 2b). Pores prepared under 15 V have 5, 6, or 7 neighbors (only 42% of pores have 6 neighbors) and obtained polygons are not symmetric (Figure 2e).

A similar tendency of pore ordering at low voltages can be observed for AAO layers obtained by anodization in sulfuric acid electrolyte. We analyze these in more detail for production of pores and nanoparticles with diameters below 20 nm.

AAO was produced in 0.3 M sulfuric acid at room temperature with anodization voltages of 20, 12, 10, and 8 V (Figure 3). The corresponding average pore diameter values are 19, 16, 13, and 11 nm, and the fraction of hexagonal cells in Voronoi diagrams were 80, 38, 45, and 44%.

dx.doi.org/10.1021/jp412689y | J. Phys. Chem. C XXXX, XXX, XXX−XXX

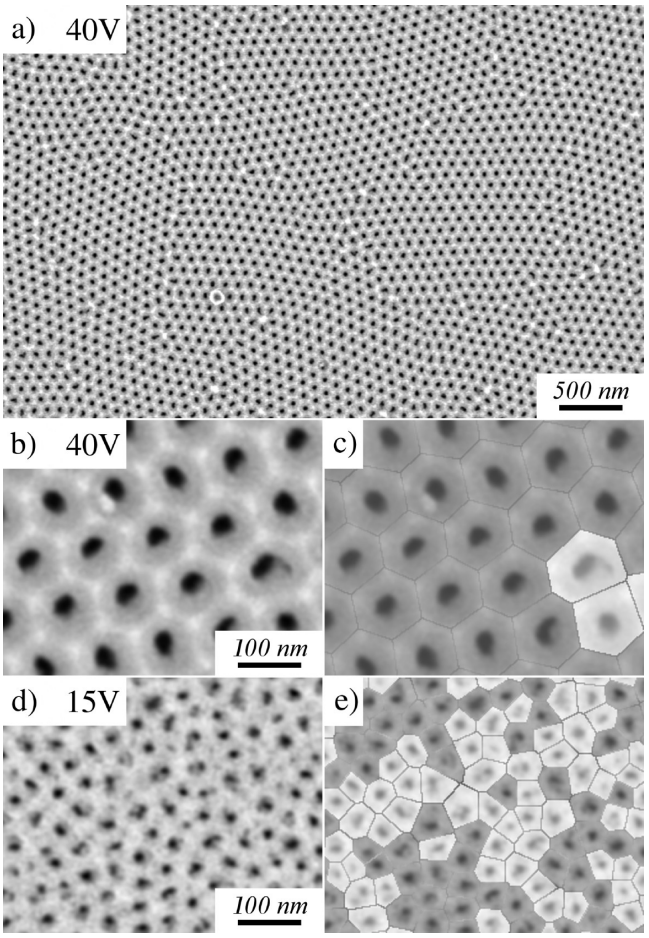

Figure 2. Top view SEM images of AAO after 45 s second anodization in 0.3 M oxalic acid using (a) 40 V (low magnification), (b) 40 V (high magnification), and (d) 15 V (anodization potential). Corresponding Voronoi diagrams (c,e) where sites surrounded by exactly six neighbors are marked by darker intensity polygons.

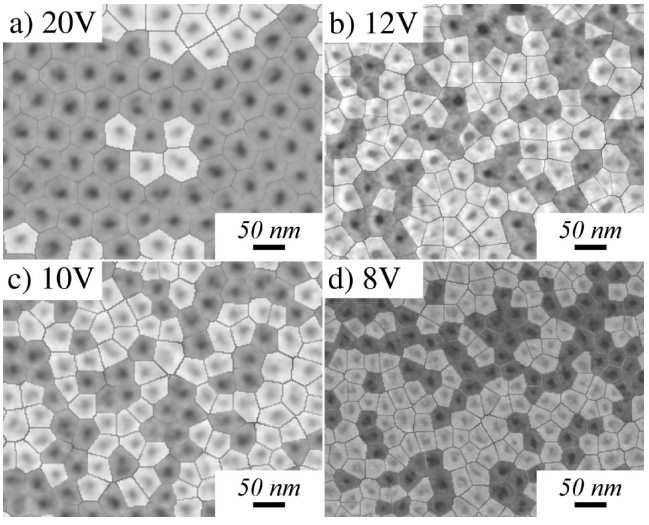

Figure 3. Top view SEM images with superimposed Voronoi diagrams of AAO layers after 45 s second anodization in 0.3 M sulfuric acid using various anodization potentials.

By comparison of AAO layers made using sulfuric and oxalic acid electrolytes, it can be clearly seen that in both cases lowering the anodization voltage decreases the regularity of pore arrangement. A similar observation was done in a recent work[24] where temperature dependence for best hexagonal arrangement of pores was determined using sulfuric acid electrolyte and anodization voltages between 15 and 25 V. This can be explained by two competing processes during anodization, namely, anodic oxide formation, which is directed by electric field, and oxide field-assisted dissolution that is less directional and strongly influenced by local perturbations near the substrate interface.

Influence of Electrolyte Concentration. Several works have addressed the role of electrolyte concentration on pore structure during anodization process.[2,6,25] In these studies the anodization time was relatively long compared to what is used in present work. It has been observed that at higher concentrations smaller pore diameters can be achieved. In search of membranes with smallest achievable pores suitable for masked deposition we produced a series of AAO layers at room temperature under constant anodization voltage of 10 V in six different sulfuric acid concentrations (Figure 4). As expected,

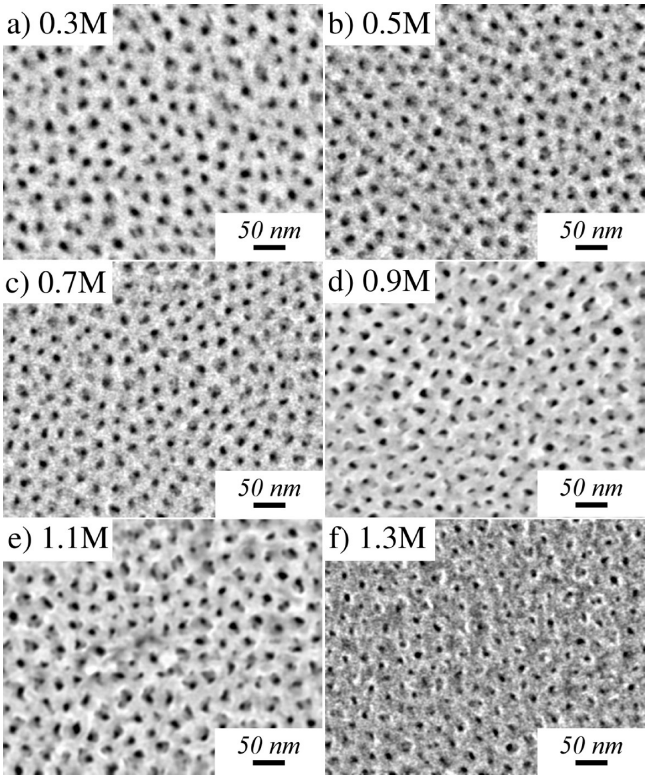

Figure 4. Top view SEM images of anodized aluminum oxide after second anodization at 10 V in different H_2SO_4 concentrations: (a) 0.3, (b) 0.5, (c) 0.7, (d) 0.9, (e) 1.1, and (f) 1.3 M.

pore diameters slightly decrease for higher electrolyte concentration (from 13 nm in 0.3 M sulfuric acid to 11 nm in 1.3 M sulfuric acid) (Figure 4g). However, the highest electrolyte concentrations are not best suited for membrane production for masked deposition as will be discussed shortly.

Transfer of Freestanding Ultrathin AAO Membranes. On the basis of methods reported in literature,[9,10] in order to prevent etching, folding and ripping of the obtained thin AAO layer during transfer process the pore surface can be covered with polymer PMMA solution after the second anodization step. Unfortunately, for the case of ultrathin membranes studied in this work such composite PMMA/AAO membrane

dx.doi.org/10.1021/jp412689y | J. Phys. Chem. C XXXX, XXX, XXX–XXX

is too flexible during residual aluminum removal in $CuCl_2$/HCl solution. Moreover, during reaction of residual Al with $CuCl_2$/HCl solution, intensive gas (H_2) production and Cu precipitation onto sample surface was observed, which causes uncontrolled local membrane movements. To reduce such local damage of membrane, we reinforced the PMMA/AAO membrane covering it with a thick layer of paraffin. Resulting paraffin/PMMA/AAO structure is more resistant to folding forces (capillary and thermal expansion) in etching liquid. As a next improvement to existing methods, we decreased Al dissolution speed by adding 10 wt % $FeCl_3$ to $CuCl_2$/HCl etching solution in ratio 3:1. Using this mixed etching solution, the length of the residual Al etching process was about 3 h for a 0.35 mm thick Al sheet. During above reaction the surface tension was reduced adding nonionic surfactant Triton X-100 to etching mixture.

The next critical step in production of ultrathin AAO membranes for masked deposition is barrier layer removal and pore opening. The composite paraffin/PMMA/AAO membrane was floated onto the surface of the 5 wt % H_3PO_4 solution. The porous structure of the thin AAO can be damaged during extended etching times because H_3PO_4 solution enters the pores and dissolves the pore walls. Our rule of thumb is to use pore opening time in minutes equal to value applied anodization voltage, for example, if anodization was done at 10 V potential then the required time to etch the barrier layer should be 10 min.

Using above-described method, we could transfer 50−100 nm thick AAO membranes prepared in sulfuric acid electrolyte. Although initial membrane area extended over 1 cm^2, inspection of surface in optical microscope revealed uniform areas without cracks or folds up to ∼100 μm across. Membranes as thin as 35 nm could be transferred but a covered area consists of small pieces (few square micrometers) of membrane. Figure 5 shows SEM images of transferred AAO membranes on a glass surface. After barrier layer etching and PMMA layer removal, pore diameters increase by 28−45% (Table 1). Moreover, membranes obtained by anodization at highest concentrations with smallest initial pore diameters did lose much of the pore wall material during barrier layer removal. This can be explained by increased concentration of sulfate ions inside pore walls that facilitate faster dissolution rate in H_3PO_4 solution. In addition, branched and paired cells with thin pore walls obtained at low anodization voltages may merge and form larger apertures during barrier layer removal. The resulting pore diameters are nearly invariant to electrolyte concentration. However, we find that the relative change in pore diameter during barrier layer removal is smallest for samples obtained using 0.7 M sulfuric acid electrolyte.

Considering above, 0.7 M electrolyte concentration yields the most stable membrane structure. Despite significant scatter in experimental data (Table 1), these membranes also have the smallest pore diameters and are considered as optimal for masked deposition of nanoparticles.

Deposition of Nanoparticle Arrays. Finally we demonstrate how AAO membranes, produced with the above method and transferred to a Si substrate, can be used as evaporation masks for nanoparticle deposition. The pore diameter 18 nm to membrane thickness 55 nm (determined by atomic force microscope) ratio is 1:3. Example of formation of Cr nanoparticles with average diameter 16 nm (standard deviation 3) and 32 nm mean distance prepared in 0.7 M sulfuric acid electrolyte under anodization voltages of 10 V is shown in Figure 6.

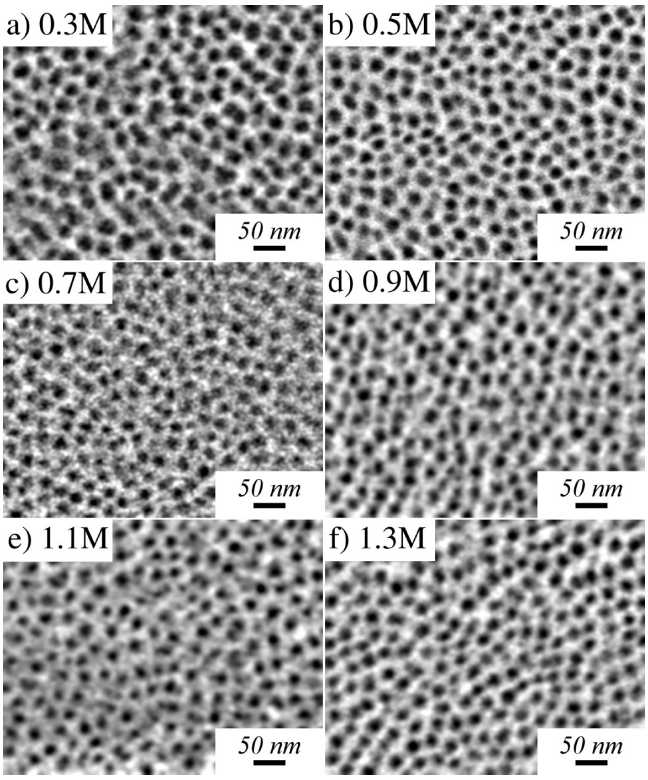

Figure 5. Top view SEM images of the AAO layer after barrier layer removal and transfer on a glass surface. Anodization of aluminum was done 10 V in different H_2SO_4 concentrations: (a) 0.3 M, (b) 0.5 M, (c) 0.7 M, (d) 0.9 M, (e) 1.1 M, and (f) 1.3 M.

Table 1. Pore Diameter after Second Anodization (D_1) and after Transfer to a Glass Surface with Removed Barrier Layer (D_2) Obtained at Various Concentrations of H_2SO_4 Electrolyte

concentration	D_1 (nm)	D_2 (nm)	rel. increase of pore diam.
0.3 M	13 ± 2	19 ± 2	32%
0.5 M	13 ± 2	19 ± 3	32%
0.7 M	**13 ± 2**	**18 ± 2**	**28%**
0.9 M	12 ± 2	19 ± 2	37%
1.1 M	11 ± 2	18 ± 2	39%
1.3 M	11 ± 2	20 ± 3	45%

The substrate and deposited material is not limited to Si and Cr. We have used the same technique to produce Ag and Au nanoparticles on glass for plasmonic applications.[16] The limiting factor for substrate material is the ability to withstand 500 °C in oxygen atmosphere during PMMA removal.

CONCLUSIONS

We have studied the diameter, arrangement, and applicability for masked deposition of AAO membranes produced in electrochemical process near lowest usable anodization voltage limit. The pore diameter on bulk Al sheet could be tuned from 11 to 19 nm using sulfuric acid electrolyte at anodization voltages 8−20 V and 16− 39 nm using oxalic acid solution at 15−40 V. Pores obtained at low-voltage anodization lose their periodic hexagonal arrangement.

dx.doi.org/10.1021/jp412689y | J. Phys. Chem. C XXXX, XXX, XXX−XXX

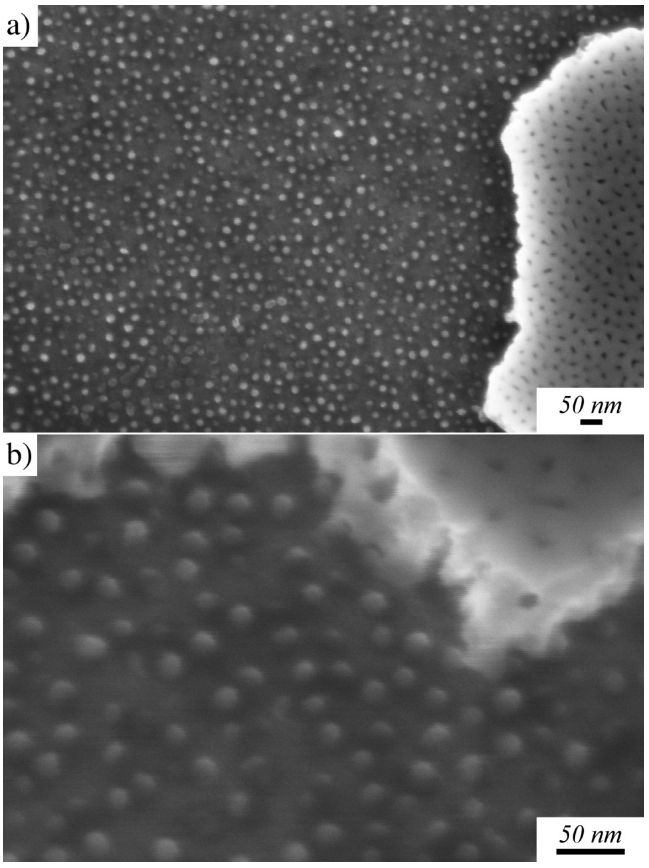

Figure 6. SEM image of arrays of Cr nanoparticles on a Si surface (a) top-view (b) sample tilted and more magnified.

We have demonstrated an improved AAO membrane transfer method of exceptionally thin AAO masks with pore diameter to membrane thickness aspect ratio 1:3−1:5. Even lower aspect ratio (1:2) membranes could be transferred at a cost of significantly reduced usable area.

As an application example, we used a transferred AAO membrane as evaporation mask and produced, metal nanoparticle arrays with average particle diameter 16 nm and average center separation 32 nm. The arrays are not periodic. However, there is a characteristic distance between nearest neighbors. This type of short-range ordered arrays has interesting optical properties[16,26] with possible applications for broad band solar energy conversion[27] or novel sensor devices.[28] The presented method allows production of exceptionally small nanoparticle arrays with high density of various materials suitable for conductive and nonconductive substrates. The particle size and shape could be further tuned by angled sputtering.

AUTHOR INFORMATION

Corresponding Author

*E-mail: donats.erts@lu.lv. Phone: +371 67033875.

Notes

The authors declare no competing financial interest.

ACKNOWLEDGMENTS

This work was done within the ERAF project 2010/0251/2DP/2.1.1.1.0/10/APIA/VIAA/096 and was supported by the Swedish Institute under the project "Complex Oxide Films and devices at the Nanoscale".

REFERENCES

(1) Masuda, H.; Fukuda, K. Ordered Metal Nanohole Arrays Made by a Two-Step Replication of Honeycomb Structures of Anodic Alumina. *Science* **1995**, *268*, 1466−8.

(2) Nielsch, K.; Choi, J.; Schwirn, K.; Wehrspohn, R. B.; Gösele, U. Self-ordering Regimes of Porous Alumina: The 10 Porosity Rule. *Nano Lett.* **2002**, *2*, 677−680.

(3) Chu, S. Z.; Wada, K.; Inoue, S.; Todoroki, S. Formation and Microstructures of Anodic Alumina Films from Aluminum Sputtered on Glass Substrate. *J. Electrochem. Soc.* **2002**, *149*, B321.

(4) Keller, F.; Hunter, M. S.; Robinson, D. L. Structural Features of Oxide Coatings on Aluminum. *J. Electrochem. Soc.* **1953**, *100*, 411.

(5) Karmhag, R.; Tesfamichael, T.; Wäckelgå rd, E.; Niklasson, G. A.; Nygren, M. Oxidation Kinetics of Nickel Particles: Comparison Between Free Particles and Particles in an Oxide Matrix. *Sol. Energy* **2000**, *68*, 329−333.

(6) O'Sullivan, J. P.; Wood, G. C. The Morphology and Mechanism of Formation of Porous Anodic Films on Aluminium. *Proc. R. Soc. London, Sect. A* **1970**, *317*, 511−543.

(7) Ono, S.; Masuko, N. Evaluation of Pore Diameter of Anodic Porous Films Formed on Aluminum. *Surf. Coat. Technol.* **2003**, *169−170*, 139−142.

(8) Mao, R. W.; Lin, S. K.; Tsai, C. S. In Situ Preparation of an Ultra-Thin Nanomask on a Silicon Wafer. *Nanotechnology* **2009**, *20*, 025301.

(9) Masuda, H.; Satoh, M. Fabrication of Gold Nanodot Array Using Anodic Porous Alumina as an Evaporation Mask. *Jpn. J. Appl. Phys.* **1996**, *35*, L126−L129.

(10) Wu, M.; Wen, L.; Lei, Y.; Ostendorp, S.; Chen, K.; Wilde, G. Ultrathin Alumina Membranes for Surface Nanopatterning in Fabricating Quantum-Sized Nanodots. *Small* **2010**, *6*, 695−9.

(11) Ding, G. Q.; Zheng, M. J.; Xu, W. L.; Shen, W. Z. Fabrication of Controllable Free-Standing Ultrathin Porous Alumina Membranes. *Nanotechnology* **2005**, *16*, 1285−1289.

(12) Lee, W.; Han, H.; Lotnyk, A.; Schubert, M. A.; Senz, S.; Alexe, M.; Hesse, D.; Baik, S.; Gösele, U. Individually Addressable Epitaxial Ferroelectric Nanocapacitor Arrays With Near Tb Inch-2 Density. *Nat. Nanotechnol.* **2008**, *3*, 402−7.

(13) Gao, X.; Rodriguez, B. J.; Liu, L.; Birajdar, B.; Pantel, D.; Ziese, M.; Alexe, M.; Hesse, D. Microstructure and Properties of Well-Ordered Multiferroic Pb(Zr,Ti)O(3)/CoFe(2)O(4) Nanocomposites. *ACS Nano* **2010**, *4*, 1099−107.

(14) Lei, Y.; Cai, W.; Wilde, G. Highly Ordered Nanostructures with Tunable Size, Shape and Properties: A New Way to Surface Nano-Patterning Using Ultra-Thin Alumina Masks. *Progr. Mater. Sci.* **2007**, *52*, 465−539.

(15) Pastore, I.; Poplausks, R.; Apsite, I.; Pastare, I.; Lombardi, F.; Erts, D. Fabrication of Ultra Thin Anodic Aluminium Oxide Membranes by Low Anodization Voltages. *IOP Conf. Ser.: Mater. Sci. Eng.* **2011**, *23*, 012025.

(16) Prikulis, J.; Malinovskis, U.; Poplausks, R.; Apsite, I.; Bergs, G.; Erts, D. Optical Scattering by Dense Disordered Metal Nanoparticle Arrays. *Plasmonics* **2013**, DOI: 10.1007/s11468-013-9639-2.

(17) Choi, Y.; Hyeon, J.; Bu, S.; Bae, T. Effects of Anodizing Voltages and Corresponding Current Densities on Self-Ordering Process of Nanopores in Porous Anodic Aluminas Anodized in Oxalic and Sulfuric Acids. *J. Korean Phys. Soc.* **2009**, *55*, 835−840.

(18) Maria Chong, A. S.; Tan, L. K.; Deng, J.; Gao, H. Soft Imprinting: Creating Highly Ordered Porous Anodic Alumina Templates on Substrates for Nanofabrication. *Adv. Funct. Mater.* **2007**, *17*, 1629−1635.

(19) *Nanostructured Materials in Electrochemistry*; Eftekhari, A., Ed.; Wiley-VCH Verlag GmbH & Co. KGaA: Weinheim, Germany, 2008.

(20) Schneider, C. A.; Rasband, W. S.; Eliceiri, K. W. NIH Image to ImageJ: 25 years of image analysis. *Nat. Methods* **2012**, *9*, 671−675.

(21) Thompson, G. E.; Wood, G. C. Porous Anodic Film Formation on Aluminium. *Nature* **1981**, *290*, 230−232.

(22) Voronoi, G. Nouvelles Applications des Paramètres Continus à la Théorie des Formes Quadratiques. Deuxième mémoire. Recherches

sur les Paralléllοèdres Primitifs. *J. Reine Angew. Math.* **1908**, *1908*, 198−287.
(23) Borba, J. R.; Brito, C.; Migowski, P.; Vale, T. B.; Stariolo, D. A.; Teixeira, S. R.; Feil, A. F. Quantitative Characterization of Hexagonal Packings in Nanoporous Alumina Arrays: A Case Study. *J. Phys. Chem. C* **2013**, *117*, 246−251.
(24) Sulka, G.; Parkoła, K. Temperature Influence on Well-Ordered Nanopore Structures Grown by Anodization of Aluminium in Sulphuric Acid. *Electrochim. Acta* **2007**, *52*, 1880−1888.
(25) Huang, Y.; Zeng, H.-y.; Zhao, C.; Qu, Y.-q.; Zhang, P. Kinetic Models of Controllable Pore Growth of Anodic Aluminum Oxide Membrane. *Met. Mater. Int.* **2012**, *18*, 433−438.
(26) Schwind, M.; Miljković, V. D.; Zäch, M.; Gusak, V.; Käll, M.; Zorić, I.; Johansson, P. Diffraction From Arrays of Plasmonic Nanoparticles With Short-Range Lateral Order. *ACS Nano* **2012**, *6*, 9455−65.
(27) Atwater, H. A.; Polman, A. Plasmonics for Improved Photovoltaic Devices. *Nat. Mater.* **2010**, *9*, 205−13.
(28) Stewart, M. E.; Anderton, C. R.; Thompson, L. B.; Maria, J.; Gray, S. K.; Rogers, J. A.; Nuzzo, R. G. Nanostructured Plasmonic Sensors. *Chem. Rev.* **2008**, *108*, 494−521.